Two-photon microscopy and spectroscopy based on a compact confocal scanning head

Alberto Diaspro
University of Genoa
National Institute for the Physics of Matter (INFM)
Department of Physics
Via Dodecaneso 33
16146 Genova, Italy

Giberto Chirico
National Institute for the Physics of Matter (INFM)
Department of Physics
Piazza delle Scienze, 3
20126 Milano, Italy

Federico Federici
University of Genoa
National Institute for the Physics of Matter (INFM)
Department of Physics
Via Dodecaneso 33
16146 Genova, Italy

Fabio Cannone
Sabrina Beretta
National Institute for the Physics of Matter (INFM)
Department of Physics
Piazza delle Scienze, 3
20126 Milano, Italy

Mauro Robello
University of Genoa
National Institute for the Physics of Matter (INFM)
Department of Physics
Via Dodecaneso 33
16146 Genova, Italy

Abstract. We have combined a confocal laser scanning head modified for TPE (two-photon excitation) microscopy with some spectroscopic modules to study single molecules and molecular aggregates. The behavior of the TPE microscope unit has been characterized by means of point spread function measurements and of the demonstration of its micropatterning abilities. One-photon and two-photon mode can be simply accomplished by switching from a mono-mode optical fiber (one-photon) coupled to conventional laser sources to an optical module that allows IR laser beam (two-photon/TPE) delivery to the confocal laser scanning head. We have then described the characterization of the two-photon microscope for spectroscopic applications: fluorescence correlation, lifetime and fluorescence polarization anisotropy measurements. We describe the measurement of the response of the two-photon microscope to the light polarization and discuss fluorescence polarization anisotropy measurements on Rhodamine 6G as a function of the viscosity and on a globular protein, the Beta-lactoglobulin B labeled with Alexa 532 at very high dilutions. The average rotational and translational diffusion coefficients measured with fluorescence polarization anisotropy and fluorescence correlation methods are in good agreement with the protein size, therefore validating the use of the microscope for two-photon spectroscopy on biomolecules. © 2001 Society of Photo-Optical Instrumentation Engineers. [DOI: 10.1117/1.1382809]

Keywords: two-photon imaging; micropatterning; photobleaching; 3-D microscopy; lifetime; fluorescence polarization anisotropy; two-photon spectroscopy; fluorescence fluctuations; point spread function.

Paper FM-03 received Mar. 20, 2001; revised manuscript received Mar. 24, 2001; accepted for publication Apr. 11, 2001.

1 Introduction

Although conceived over 20 yr[1,2] ago and developed in its modern form 10 yr ago,[3] two-photon excitation (TPE) fluorescence microscopy can be considered a comparatively young technique in far-field fluorescence optical microscopy, taking advantages over both wide field and confocal laser scanning microscopy (CLSM),[4–7] for the study of the three-dimensional (3D) and dynamic properties of biological systems.[8–13]

Moreover, a comparatively new form of spectroscopy, related to the use of tiny excitation volumes, has grown together with the development of confocal and two-photon excitation microscopy. In fact, the advent of two-photon excitation microscopes has fostered the application of techniques such as fluorescence correlation spectroscopy (FCS)[14–17] or fluorescence lifetime to single biological molecules and to the characterization of tissues.[18–23]

It is worth noting that the development of mode-locked lasers, providing moderate average power at high repetition rates and ultrafast pulses,[24–26] matched with the increased dissemination of confocal laser scanning microscopes, favored an incredible increase of demands for developing TPE architectures. It is our opinion, that the simplest and fastest method for implementing two- or multiphoton excitation microscope is to modify a commercial CLSM. Less inviting alternatives are to modify a common optical microscope or to buy a commercial TPE microscope.[27,28]

There are two popular approaches to realize TPE imaging architectures based on a CLSM, namely: descanned and non-descanned mode.[29,20,30–35,28] The former uses the very same optical pathway and mechanism employed in CLSM. Pinholes are removed or set to their maximum aperture and the emission signal is captured using the galvanometric scanning mirrors. In order to obtain a better spatial resolution it is also possible to keep confocal pinholes, also considering a right balance between spatial resolution and detection sensitivity.[36,37] When pinhole insertion is possible, the major advantage is attained in terms of axial resolution that can be ameliorated approximately of the 40%.[38]

The latter approach allows a significant signal-to-noise ratio increase. The signal is collected using dichroic mirrors on the emission path or external detectors without passing through the galvanometric scanning mirrors. Unfortunately, this approach introduces some problems related to external detectors positioning and environmental light noise. This means that it is not immediate as the descanned solution. Be-

side the imaging capabilities of a two-photon setup that exploits directly the fluorescence output, we also consider images of the samples obtained through mapping of other spectroscopic properties, such as the decay time of the excited states or the relaxation rate of the fluctuation of fluorescence. These properties can be studied in a point-by-point way on a solid sample (for example a tissue) thereby reconstructing an image,[20,23] or in solution with a laser beam kept at a fixed position and waiting for the molecules to pass through the excitation volume.[14,17] We will refer in the following to this second type of spectroscopic application. Fluorescence correlation spectroscopy is a very sensitive tool to investigate a variety of properties of biomolecules in solutions, from translational and rotational diffusion to chemical reactions.[15,39,40] Confocal detection with low power continuous wave (cw) laser sources is usually adopted to achieve the small excitation volumes needed for the study of the fluorescence fluctuations.[41–43] More recently two-photon (and multiphoton) excitation with pulsed infrared (IR) lasers has been exploited to enhance the background rejection and reduce the excitation volumes with respect to the more conventional single-photon confocal techniques.[3,20] In both cases the time dependence of the fluorescence has been widely characterized by means of correlation methods. The analysis of the autocorrelation function of the fluorescence signal as detected by a photomultiplier tube (PMT) or an avalanche photodiode (APD), gives two main parameters, the average number of molecules in the excitation volume $\bar{N}$ and the molecular translational diffusion coefficient D.[44]

The probability distribution of the photon counting can be used, beside correlation functions, for the description of random processes[45] but it has generally received less attention than the correlation methods. Theoretical and experimental studies[44] have recently shown how to extract detailed information on $\bar{N}$ and the molecular brightness ϵ from the photon counting histogram (PCH). This theoretical treatment implements the previous ones[46] by taking explicitly into account the shape of the point spread function (PSF) and the motion of the tracer molecule. The experimental test has showed that this approach can also be applied to a mixture of species characterized by different quantum yields.[47]

2 TPE Architecture: General Considerations

2.1 Microscopy

The main components for TPE microscopy are almost identical to those of CLSM but some sagacity has to be used.[28,27,48] Currently, the mode-locked Ti: sapphire laser[25] is the preferred source, also for the small amplitude fluctuations produced that could become critical in a TPE application where the fluorescence intensity depends on the square of the excitation intensity. Moreover, the trend of the market is to produce compact and easy to use mode-locked lasers and this fact not only reduces the cost and problems related to maintenance but also the complexity of the operations related to laser functioning and the room needed. The features of infrared pulsed laser are high average power, 80 MHz high repetition rate, and 100 fs short pulse width. The use of short pulses and small duty cycles is mandatory to allow image acquisition in a reasonable time while using power levels that are biologically

tolerable.[49–51] A suitable laser source, to take advantage of any available fluorescent molecule, should also be widely tunable. The average power outputs are commonly in excess (200 mW–1 W) and allow therefore to serve different instruments at the very same time.

The laser beam can be directly coupled to the scanning head, enclosures, and boxes should be used to allow safe operations. Some research groups are working on optical fiber coupling and different commercial systems are available for femtosecond and picosecond operating laser sources. However, some problems and drawbacks still remain.[52]

In principle, any confocal scanning unit can be converted to a TPE microscope.[8,7] In practice, one needs the simplest confocal unit, optically speaking. The best solution is a confocal scanning head with a very reduced optical path and requiring easy manual operations for controlling dichroic positions, pinhole aperture, and excitation power. The different excitation wavelengths require replacement of a dichroic beam splitter that usually is inserted in any confocal unit and that separates fluorescence from excitation. In terms of filters, changes have also to be done in the output module where fluorescence is collected. In fact, the excitation of light needs to be suppressed by 6–10 orders of magnitude.[53] The test can be performed by recording images from large fluorescent spheres or films of fluorescent molecules at different power levels to check for quadratic power behavior. If it is less than two some reflections are affecting the acquisition. Scanning mirrors should be metal coated (silver) and should have a good thermal resistance.[27]

2.2 Spectroscopy

Spectroscopy applications can be performed either on a tiny volume fixed on the sample plane or by performing the spectroscopic measurement while scanning the sample. The former is preferred for studies of the heterogeneity of molecular solutions[47] or of the binding of different fluorescent species, while the latter allows obtaining lifetime imaging of the tissues (FLIM). In any case one of the main problems is again the rejection of the stray scattering light since it lowers the fluorescence fluctuation and the efficient detection of the low fluorescence levels involved in these studies. A part from the use of high rejection filters for the IR light, the use of high quantum yield detectors with low noise equivalent power (NEP) is the crucial issue for this point. The best detectors at the moment are avalanche photodiodes that have NEP $<10^{-15}$ W/Hz$^{0.5}$ for a 0.5 mm diode area and at least 70% quantum yield at 630 nm.[54] A second relevant issue in the design and the use of a two-photon excitation or confocal setup for spectroscopy is the full characterization of the excitation volume that greatly determines the relaxation time of the fluorescence fluctuations. The fluorescence signal detected through an optical setup can be expressed as the product of the fluorophore concentration in the object plane times the detection efficiency function[42] that can be taken as an effective laser profile. As a matter of fact, in order to quantitatively apply fluorescence fluctuation spectroscopy, one must have a detailed knowledge of the shape of this effective excitation laser profile. In an ideal confocal setup, obtained for an infinitesimal size of the detection pinhole, this function is given by the square of the PSF of the objective,[55] and for a finite size of the pinhole, this limiting PSF must be convolved to the trans-

mission function of the pinhole.[4,56] The effective excitation laser profile in a confocal setup has been the object of several theoretical and experimental works and it is assumed to have a Gaussian shape both in the object plane and in the optical path direction. So far, in a TPE architecture the excitation of the fluorescent molecules occurs because of the nonlinear response of the molecules to the electric field. It is common to assume that the effective excitation profile is simply given by the square of the (Gaussian–Lorentzian) laser beam focused by the objective. The estimate of the laser beam waist is usually obtained by measuring the fluorescence correlation function of a known dye. Both the decay time of this function and the signal-to-noise ratio are related to the excitation volume. However the estimate of the signal-to-noise ratio from the fluorescence correlation function is a delicate matter due to the contribution of shot noise, of retarded fluorescence, and of uncorrelated background to the short lag time part of the correlation decay.

In Sec. 3 we give examples of the characterization of the excitation volume and a comparison to the PSF determined on the imaging path of the microscope. This is made by the analysis of the fluorescence correlation and of the photon counting histogram (PCH) method and by studying the dependence of the measured excitation volume on the laser beam diameter. The PCH method allows measuring the excitation volume without resorting to the *a priori* knowledge of the diffusion coefficient of the observed tracer molecule.

3 An Example of Realization of Multipurpose TPE Architecture

This section is related to the realization of a TPE microscope for imaging and spectroscopy applications achieved through minor modifications of a commercial CLSM, in which the ability to operate as a standard CLSM has been preserved.[10,57] A panoramic view of the experimental setup is given in Figure 1(a).

The core of the architecture is a mode-locked Ti:sapphire infrared pulsed laser (Tsunami 3960Spectra Physics Inc., Mountain View, CA, USA), pumped by a high-power (5 W @ 532 nm) solid state laser (Millennia V, Spectra Physics Inc., Mountain View, CA, USA). The Ti:sapphire laser output can be tuned across a range from 680 to 830 nm, with a bandwidth from 4 to 12 nm, allowing excitation of a variety of fluorescent molecules normally excited by visible and ultraviolet radiation.[58,59] The restriction of the tunable range is given by the set of mirrors installed for our purposes. A dichroic mirror, optimized for high power ultrashort infrared pulses (CVI, USA), is used to bring in air the Tsunami beam to the scanning head. Before entering into the scanning head, beam average power is brought to values ranging from 2 to 50 mW using a neutral density rotating wheel (Melles Griot, USA). For an average power of 20 mW at the entrance of the scanning head, the average power before the microscope objective is about 9–13 mW and at the sample is estimated between 3 and 5 mW. At the focal volume a 1.5–2. times broadening occurs using a high numerical aperture objective and a reduced amount of optics within the optical path.[32,60,61] The scanning and acquisition system for microscopic imaging is based on a commercial single-pinhole scanning head Nikon PCM2000 (Nikon Instr., Florence, Italy) mounted on the lat-
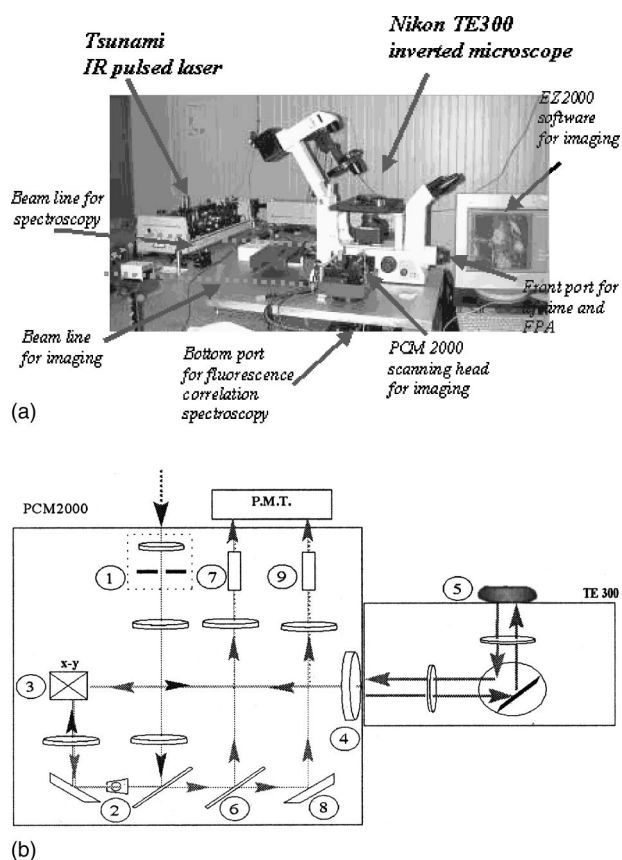
Fig. 1 (a) Photograph of TPE microscope operating at the laboratory of physics of biosystems (LFB, Department of Physics, University of Genoa, Italy), within the strategic framework of a national project of the National Institute for the Physics of Matter (INFM; http://www.infm.it). This microscope, realized in 1999, is part of a multipurpose architecture including also lifetime imaging and fluorescence correlation spectroscopy modules (see Ref. 7). (b) This simplified optical scheme outlines the components of the confocal scanning head Nikon PCM2000. The excitation beam enters into the scanning head through a coupling lens (1) in order to reach the sample on the *x-y-z* stage (5). The beam passes through the pinhole holder (2) kept in open position, the galvanometric mirrors (3) and the scanning lens (4) that optically couple the beam to the microscope objective. Fluorescence coming from the sample (5) is directed to the acquisition channels by two selectable mirrors (6), (8) via optical fiber (7), (9) coupling (see Ref. 35).
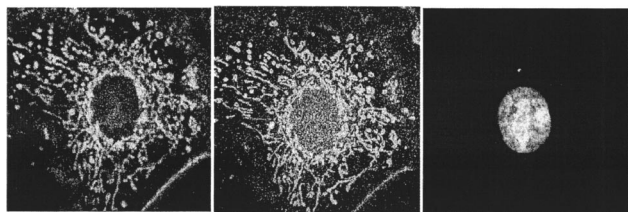
eral port of a common inverted microscope, Nikon Eclipse TE300. Ths scanning head has a simple and compact light path that makes it very appropriate for conversion to a two-photon scope.[62,28] Figure 1(b) outlines in a somplified scheme its optical design. The optical resolution performances of this microscope when operating in conventional confocal mode, and using a $100\times/1.3$ NA oil immersion objective, have been reported in detail elsewhere and are 178 ± 21 nm laterally and 509 ± 49 nm axially.[63] The scanning head operates in the "open pinhole" condition.

A series of emission custom made filters, that block infrared radiation (>650 nm) to an optical density of 6–7 within 50 mW of beam power incident on the filters themselves, are employed.[53] In particular, the E650P filter (Chroma Inc., Brattleboro, VT, USA) constitutes the base for the other emission filters.

One-photon and two-photon modes can be simply accomplished by switching from the single-mode optical fiber (one photon), coupled to a module containing conventional laser sources (Ar-ion, He–Ne green), to the optical path in air, delivering the Tsunami laser beam (two photon), as shown in Figure 2. A high throughput optical fiber delivers the emitted fluorescence from the scanning head to the PCM2000 control unit where PMTs (R928, Hamamatsu, Japan) are physically plugged. Axial scanning for confocal and TPE three-dimensional imaging is actuated by means of two different positioning devices, namely: a belt driven system using a dc motor (RFZ-A, Nikon, Japan) and a single objective piezo-electric nano-positioner (PIFOC P-721-17, Physik Instrumente, Germany). Acquisition and visualization operations are completely computer controlled by a dedicated software, EZ2000 (Coord, The Netherlands; http://www.coord.nl). The main controls are related to PMTs voltage, pixel dwell time, frame dimensions (1024×1024 maximum), field of scan (from 1 to 140 μm using a $100 \times$ objective).

For the spectroscopy applications the laser beam (30% of the output power) is deviated by a beamsplitter just in front of the laser output and is sent to the rear port of the microscope by a beam steering, see Figure 1(a).[57] The laser power at the object plane can be set by means of neutral filters. In order to achieve the smallest volumes we must expand the laser beam in order to fill almost completely the entrance pupil of the objective. We have found it is almost equivalent to expand the laser beam two or three times right at the entrance of the microscope with a beam expander, or to steer the beam along a longer path on the optical bench with a couple of fast mirrors and let the beam expand because of its intrinsic divergence. In both cases the beam reaches a diameter of approximately 3 mm which almost fills the entrance pupils of the employed objectives. The use of the beam expander should deteriorate the pulse width of the laser with respect to the use of fast mirrors, however we have not detected an appreciable difference in the fluorescence output with the two methods.

The laser light is then reflected by a dichroic mirror (650 DCSPRX C72-38, Nikon, Japan) mounted on the dichroic holder sleeve of the TE300 microscope, and focused on the sample with a $100 \times$ oil objective (NA$=1.4$, Plan Apochromat DICH $100 \times$ oil, working distance 0.19 mm, focal length

2 mm, Nikon, Japan). The fluorescence emission is collected by the same objective, passes through the dichroic mirror and through a band pass filter (depending on the fluorophore emission; for fluoresceine we use a HQ535/50, Chroma, VT, U.S.A.) to diminish the red and infrared light reflected toward the detector that is mounted on the bottom or the front ports. On the bottom port we detect it in single photon counting mode for the FCS applications, while on the front port we use an analog detector for the measurements of lifetimes and fluorescence polarization anisotropy decays. For single photon counting detection we have used a R928 PMT (Hamamatsu, Japan) and an avalanche photodiode (APD) (SPCM-AQ-151, EG&G, Wellesley, MA) finding that the performance of the APD is by far the best for the FCS application on highly dilute samples at low excitation power. This is probably due to the difference in the NEP of the two detectors and in the higher quantum yield of the APD compared to the photomultiplier ($\cong 10\%$). The measurements shown in the following have been collected with the APD.

For the FCS measurements, the APD output is digitized by a photon counting module (ALBA, ISS, Urbana-Champaign, IL) and the TTL pulses are acquired by a 40 MHz acquisition board (ISS, Urbana-Champaign, IL). The correlation functions of the fluorescence fluctuations are computed online by the acquisition software and the raw data, i.e., photon counts per sampling time versus acquisition time, are stored and analyzed offline to obtain the PCHs.

For the time resolved fluorescence measurements (lifetime or polarization anisotropy) the fluorescence light is detected through the front port of the microscope (180° with respect to the excitation beam direction) by a photomultiplier tube (R928, Hamamatsu, Bridgewater, NY), whose gain was modulated by biasing the second dynode stage at a radio frequency $\nu_n + 360$ Hz, with $\nu_n = n \times 80$ MHz. The PMT signal is fed to an ISS lock-in amplifier board (ISS, Champaign, IL) for the measurement of the polarized modulation ratios and the phase differences of the fluorescence light with respect to the excitation laser beam. The synchronization is performed by a Lock-to-Clock system (model 3930, Spectra Physics, CA) which takes as a reference the signal of a fast diode detecting a small portion of the laser light. The 10 MHz output of the Lock-to-Clock is used as a frequency reference by the ISS board and for the synthesizer (Marconi Instruments, model 2023A, UK) that provides the rf bias for the modulation of the PMT gain. The polarization of the fluorescence is selected by means of a Glan–Thompson polarizer (extinction ratio $<10^{-6}$, Bernardt-Halle, Berlin), and the fluorescence measurements are taken with the polarizer at the magic angle[18] of 54.7°. The reference sample for the lifetime measurements is a basic solution (pH$\cong 8$) of Fluoresceine (Fluka Chemika, Cat. No. 46955), whose lifetime[64] is $\cong 4.05$ ns. The fluorescence anisotropy measurements are taken by rotating the polarizer between the directions parallel and perpendicular to that of the excitation light; the differential phase shifts and the polarized modulation ratios are now the ones of the fluorescence detected with parallel polarization taken with respect to the perpendicular component.

For each harmonic of the laser repetition frequency a minimum of one and a maximum of five differential measurements are performed in order to obtain a differential phase shift error <0.2 and a polarized modulation ratio error <0.004. For each

Fig. 2 Confocal and TPE imaging of bovine pulmonary artery endothelial cells (F-147780, Molecular probes, Oregon) marked with Mito Tracker red, Bodipy FL phallacidin and DAPI specific for mithocondria, F-actin and DNA, respectively. Confocal imaging (left) has been performed at 488 and 543 nm, TPE imaging (middle, right) has been performed at 720 nm. The images have been acquired by switching from confocal to TPE mode using a simple optical attachment for the PCM2000 scanning head developed in our laboratory, and demonstrate the maintenance of positioning when switching from one mode to another (see Ref. 7).

measurement a minimum of 20 to a maximum of 120 acquisitions are taken each corresponding to a single wave form (period $\cong 2.78$ ms); the integration time per measurement is therefore $\cong 55-330$ ms.

3.1 TPE Microscope Behavior

3.1.1 Imaging

Point spread function (PSF) measurements are referred to a planachromatic Nikon 100×, 1.4 NA immersion oil objective with enhanced transmission in the infrared region. Blue fluorescent carboxylate modified microspheres 0.1 μm diameter (F-8797, Molecular Probes, OR) were used. A drop of dilute samples of bead suspensions was spread between two coverslips of nominal thickness 0.17 mm. These microspheres constitute a very good compromise toward the utilization of sub-resolution point scatterers and acceptable fluorescence emission. An object plane field of 18 μm×18 μm was imaged in a 512×512 frame, at a pixel dwell time of 17 μs. Axial scanning was performed and 21 optical consecutive and parallel slices have been collected at steps of 100 nm. The $x-y$ scan step was 35 nm. The scanning head pinhole was set to open position. The 3D data sets of several specimens were analyzed. The measured full width at half maximum (FWHM) lateral and axial resolutions were 210±40 and 700±50 nm, respectively.[10] In order to be sure of operating in the TPE regime the quadratic behavior of the fluorescence intensity versus excitation power was also demonstrated. Another interesting issue is given by the demonstration of the localized photobleaching as compared with the single-photon confocal case. Large fluorescent microspheres (i.e., 22 μm diameter) can be used in a three-dimensional acquisition session. Figure 3(a) shows a three-dimensional selective photobleaching in the case of one-photon confocal (left side) and two-photon (right side) imaging modes. Photobleaching has been produced performing a zoom on a 1.96 μm^2 squared area appreciatively in the center plane of the microsphere. Then three-dimensional imaging has been performed using confocal and TPE mode. The resulting images are intended only for qualitative comparison and the selective bleaching can be useful to have a better feeling with respect to the power commonly used. From Figure 3(a), in the case of confocal imaging it is possible to see a double-cone-like image according to imaging conditions occurring in confocal microscopy[4,3,65,5] produced within the bead while in the TPE case the dark volume is extremely localized,[29,33,66,67] demonstrating the main difference between these two three-dimensional imaging methods: it must be remembered that in confocal imaging, even though out of focus fluorescence is not detected, it is generated. Figure 3(b) shows a writing application of the TPE microscope. Figure 4 shows a TPE image of Saccharomices cerevisiae cells marked with DAPI. This image conjugates the autofluorescence of the sample with the DAPI–DNA fluorescence coming from the nucleus. In this figure imaging is coupled to active actions like the removal of cell layers increasing the power of the beam and residence time.

3.1.2 Spectroscopy

Here, the excitation volume is measured from the diffusion of yellow–green fluorescent latex microspheres of diameter 64

(a)

(b)
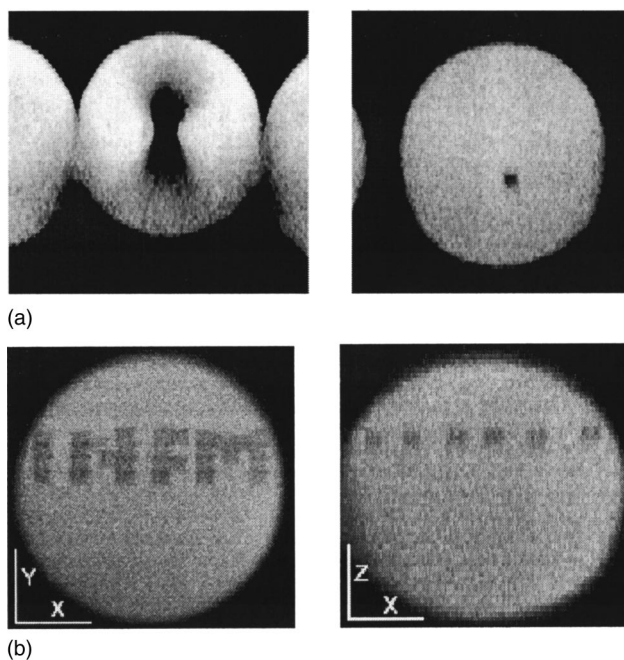
Fig. 3 (a) Three-dimensional $x-z$ projections of induced photobleaching within a large fluorescent sphere made in single-photon confocal (left) and TPE (right) mode. In confocal mode 488 nm laser beam has been used both for photobleaching and imaging keeping the pinhole at its smallest size. In TPE, 720 nm excitation wavelength has been used, at 10 mW average power. In both cases 3 μs dwell time has been used for bleaching and for imaging and a 0.5 μm axial step has been performed producing 128 optical slices. (b) Localized photobleaching used for writing in the central plane of a 22 μm sphere the characters INFM, as shown in the $x-y$ and $x-z$ views.

±9 nm (Polysciences, Fluoresbrite YG, Cat. No. 17149) suspended in de-ionized and filtered (0.22 μm, Millipore filter) water. It is essential that the concentration obtained by dilution from the mother solution (corresponding to $\cong 400$ nM), is determined by light absorption after filtering with a 0.22 μm Millipore filter. The absorbance has been measured by getting rid of the scattering contribution. All the measurements reported hereafter have been performed at room temperature. The fluorescence correlation function $g_F(t) = \langle \delta F(t) \delta F(0) \rangle / \langle F(0) \rangle^2$ for two photon excitation involves
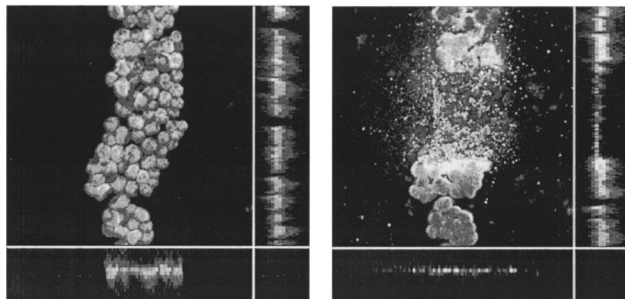
Fig. 4 Three-dimensional images ($x-y$ central, $x-z$ bottom, $y-z$ lateral views) of layers of Saccharomyces cerevisiae cells obtained in TPE mode exploiting autofluorescence. Some layers of the intact sample (left) have been destroyed (right) using localized two-photon absorption.

the numerical computation of a one-dimension integral,[68] however it can be accurately described by a simpler form of the type

$$g_F(t) = g_F(0)(1 + t/\tau)^{-1}, \qquad (1)$$

as it is shown in Figure 5 for the case $\lambda_{exc} = 770$ nm and $w_0 = 0.5 \mu$m. The extrapolation at $t = 0$ is $g_F(0) = \kappa/N_{EXC}$, where the contrast factor is $\kappa = 0.076$, and the number of molecules is related to the number concentration $\langle C \rangle$, and the volume of the excitation profile $V_{EXC} = \pi w_0^4/\lambda$ by $N_{EXC} = V_{EXC}\langle C \rangle$. The relaxation time obtained from the fit depends on the laser beam waist and the dye diffusion coefficient as $\tau = \alpha w_0^2/(8D)$, where $\alpha = 1.15 \pm 0.02$.[57]

As an example of the analysis of the FCS measurements, we show results taken at various the excitation powers in the range $1.3 < P < 7$ mW (at the entrance of the objective). The best fit parameters, $g_F(0)$ and τ are reported in the upper panel of Figure 6. The behavior of $g_F(0)$ in Figure 6 is due to the increasing effect of the uncorrelated background b_g with decreasing powers and can be accounted for by the relation[16] $g_F(0) = (\kappa/V_{EXC}\langle C \rangle)(\langle F \rangle - b_g)^2/\langle F \rangle^2$, where the dependence on the power P is in the total fluorescence rate $\langle F \rangle$ which scales as P^2, and in the background b_g, which scales as P. The average fluorescence rate $\langle F \rangle$ is a measured quantity and the background level is fit to a trend of the type, $b_g = b_{g0} + \beta P$. The best-fit curve is shown in the upper panel of Figure 6 and corresponds to $g_0 = 0.29 \pm 0.008$, $b_{g0} = 135 \pm 10$, and $\beta \cong 0.1$ Hz/mW. The measured relaxation time does not vary appreciably and is constant $\tau = 3.1 \pm 0.3$ ms. From this value we can give a first estimate of the laser beam waist w_0 by exploiting the relation $\tau = \alpha w_0^2/(8D)$ with $\alpha \cong 1.15$. The diffusion coefficient of the microspheres $D = 7.45 \mu$m^2/s is computed according to their nominal radius $R = 32$ nm, at $T = 25$ °C and by employing this value we find $V_{EXC} = \pi w_0^4/\lambda = 0.11 \pm 0.04$ fL. On the other hand, from the $g_0 = 0.29 \pm 0.008$ value and $\langle C \rangle \cong 4$ nM we can compute $V_{EXC} = \kappa/(g_0\langle C \rangle) = 0.11 \pm 0.005$ fL, in very good agreement with the estimate obtained from the relaxation time.

A further important test of the two-photon setup for spectroscopy applications is the study of the dependence of the excitation volume on the beam diameter at the entrance pupil of the objective. We give an example of such an analysis in Figure 7, where a power law fit to the data is reported as a solid line on the data of the excitation volumes obtained with the analysis reported in the previous section at various values of the beam expansion. We can write[57] the relation between V_{EXC} and the beam expansion N as $V_{EXC} = \pi\lambda^3(0.61/nN)^4((f/\Phi_0)^2 + N^2)^2$. If the ratio $f/\Phi_0 \gg N_{max} = 3$, the previous equation becomes

$$V_{EXC} \cong \pi\lambda^3(0.61/n)^4(f/\Phi_0)^4 N^{-4}. \qquad (2)$$

The power law best fit of the data in Figure 7, $V_{EXC} = (4.8 \pm 0.9)N^{-(3.9 \pm 0.3)}$ fL, gives an exponent very close to the expected fourth power. We can also estimate the laser beam radius at the entrance of the beam expander, $\Phi_0 = 0.63 \pm 0.07$ mm, by substituting the focal length of the objective, $f = 2$ mm, and the oil refraction index, $n = 1.517$ in the rela-
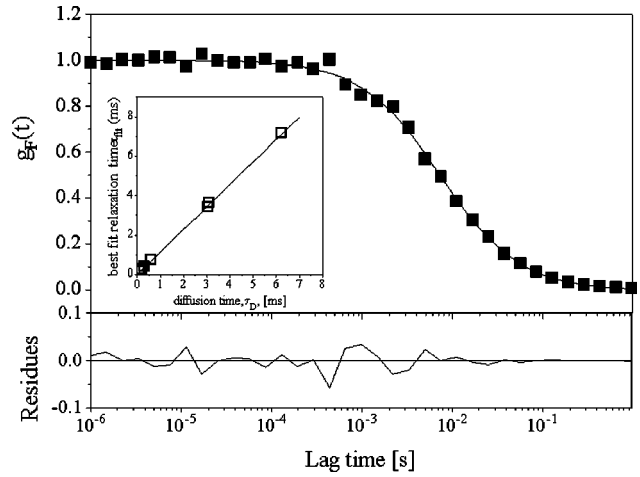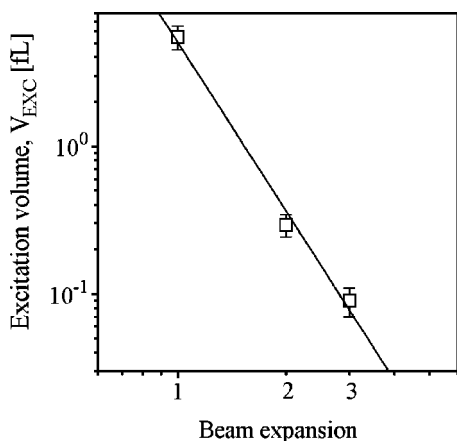

Fig. 5 Simulation of the autocorrelation function for two-photon excitation for a beam waist $w_0 = 0.5 \mu$m, $\lambda_{exc} = 770$ nm, and diffusion coefficient $D = 1 \mu$m^2/s, according to the numerical expression reported by Berland et al. (see Ref. 68). A Gaussian error (0.3%) has been added to the simulated data. The solid line represents the best fit to Eq. (1) and residues of the fit are shown in the lower panel. Inset: Best fit relaxation time obtained from the fit of the simulated autocorrelation function for two-photon excitation for different diffusion times to Eq. (1). The diffusion time is computed as $\tau_D = w_0^2/(8D)$. The linear best fit curve corresponds to a slope = 1.15 ± 0.02.

tion $(\pi\lambda^3)(0.61/n)^4(f/\Phi_0)^4 = 4.8 \pm 0.9$ fL. This value of Φ_0 is in good agreement with the Ti: sapphire laser specifications (beam radius at $1/e^2$ is <1 mm).

How robust are these methods for the determination of the excitation volume? Undesired aggregation can affect both methods since we are basically counting the number of inde-
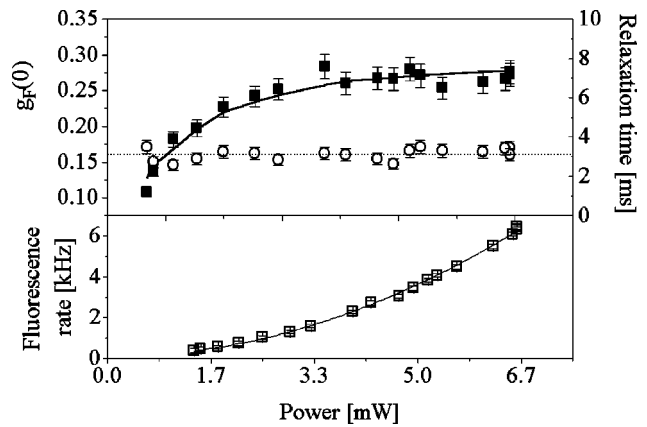

Fig. 6 (Lower panel) Fluorescence rate vs the excitation power at the entrance of the microscope. The solid line is a square law fit: $B + A(\text{power})^\nu$. The background is $B = 100 \pm 40$ Hz and the exponent is $\nu = 2.06 \pm 0.07$. (Upper panel): Best fit parameters of the correlation functions according to Eq. (6). The solid squares (left axis) indicate the $g_F(0)$ and the open circles (right axis) the relaxation times, τ. The solid line is the best fit of the $g_F(0)$ to the function $g_F(0) = g_0(\langle F \rangle b_g)^2/\langle F \rangle^2$, where $\langle F \rangle$ is the average fluorescence rate and b_g is the background rate which is assumed to depend linearly on the excitation power: $b_g = b_{g0} + \beta P$. The best fit values are $g_0 = 0.29 \pm 0.008$, $b_g = 135 \pm 10$ Hz, and $\beta = 0.1$. The dashed line indicates the average value of the relaxation time $\langle \tau \rangle = 3.1$ ms.

Fig. 7 Measurements of the excitation volume vs the beam expansion as measured from the analysis of the autocorrelation functions and the photon counting histograms. The solid line is a power law fit. The best fit exponent is -3.9 ± 0.3 (see also the text).

pendent fluorescence entities. Even after extensive filtering of the samples one finds a small fraction of aggregates, which however could be easily picked out of the averages. This is shown for example in Figure 8, where we plot the PCH computed on a single 1.6 s trace in which one observes a huge fluorescence peak (see inset) and from which a double peaked histogram is computed (see filled squares in Figure 8). In the same plot, for comparison, we report the PCH computed on a second 1.6 s trace where no huge peaks are detected and the histograms are of the same type as those analyzed in the previous paragraphs. The anomalous behavior shown in Figure 8 is very likely due to the passage of aggregates through the excitation volume. Such events, however, are very rare indicating that the number of aggregates is rather low and the measurements affected by aggregates can be singled out by looking at the average rate of each measurement.
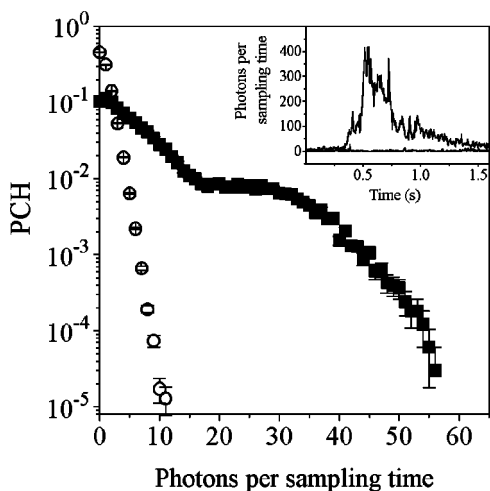
Fig. 8 Distribution of photon counts for a $C = 1.2$ nM solutions of microspheres collected for 20 kHz of sampling frequency corresponding to 50 μs of sampling time. Open circles refers to the histogram computed on a trace where no evidence of aggregates is found (lower line of the inset) and filled squares refer to the histogram of a trace where large ones are find (higher line of the inset).

A second and more critical experimental issue that can be attacked by looking at the fluorescence fluctuations, is whether the laser beam at the object plane is well shaped, i.e., it follows a Gaussian–Lorentzian shape. We have to this purpose performed a series of measurements versus the sample concentration in a case when approximately half of the laser beam cross section (which was expanded three times) was blocked at the entrance of the microscope by a misplaced diaphragm. The analysis of the auto correlation functions (ACFs) gives reasonable results although the residuals always indicate the presence of a second fast component that was more evident at higher sample concentrations (data not shown). If we force fit the ACFs to Eq. (1), the dependence of the $g_F(0)$ and the relaxation time τ upon the concentration is in reasonable agreement with the expected laws, i.e., $g_F(0)$ decreases with the concentration and τ is approximately constant (data not shown). However the estimate of the excitation volume from these two data sets disagree significantly, since $V_{\text{EXC}} = 0.5 \pm 0.05$ fL, from the $g_F(0)$ analysis, and $V_{\text{EXC}} = 0.26 \pm 0.05$ fL from the relaxation time. These values are sensibly larger than the result found when no perturbation of the laser cross section was present, $V_{\text{EXC}} \cong 0.1$ fL. It must be noted that beside the larger value of the excitation volume, the expectations of the theoretical trends of the best fit parameters are not fulfilled when the beam cross section is perturbed.

3.1.3 *Two-Photon Lifetime Decays*

A single component model can satisfactorily analyze the lifetime decays for the Rhodamine 6G (Fluka Chemika, Cat. No. 83698) solutions to give a lifetime $\tau_F = 3.95 \pm 0.2$ ns. The two quantities measured are the phase shifts and the demodulation ratios at the harmonics of the laser repetition frequency $\cong 80$ MHz. These data were fit versus the frequency by a two-exponential decay scheme using the GLOBALS UNLIMITED software,[69] in order to obtain the fluorescence lifetimes of the fluorophore. We can also show as an example of protein studies, the fluorescence decay of the Alexa dye (succymidil-esther derivative by Molecular Probes) bound to the Beta-lactoglobulin B (Sigma Chemical Co., Cat. no. L-8005, Lot. No. 13H7150) where a double exponential decay is found. The main decay component corresponds to a lifetime $\tau_F = 3.4 \pm 0.4$ ns, and there is a tiny amount ($<1\%$) of a faster decay ($\cong 0.4$ ns).

3.1.4 *Microscope Polarization Response and Fluorescence Polarization Anisotropy*

Two anisotropy components are often needed to satisfactorily interpret the differential phase shifts and polarized demodulation ratios. We ascribe these decays to the same fluorophore according to the time domain form:

$$r(t) = r_W \exp(-t/\tau_W) + r_{\text{ROT}} \exp(-t/\tau_{\text{ROT}}), \quad (3)$$

where τ_W is the libration time of the fluorophore in the binding site, τ_{ROT} is the rotational time, and r_W and r_{ROT} are the limiting anisotropies of the two components. From τ_{ROT} we obtain the rotational diffusion coefficient[70] $D_{\text{ROT}} = (6\tau_{\text{ROT}})^{-1}$. The anisotropy shape of the molecules must be taken into account for a correct interpretation of the rotational times. However, an apparent radius can be assigned by inverting the Stokes–Einstein equation

$$R_{eq}^3 = k_B T / 8\pi \eta D_{ROT}, \tag{4}$$

where k_B is the Boltzmann constant, T is the absolute temperature, and η is the solvent viscosity. All measurements were made at $T = 22.5\,°C$.

In order to measure the fluorescence polarization anisotropy (FPA) it is essential to correctly measure the components of the fluorescence intensity with polarization directions parallel $I_\parallel$ and perpendicular $I_\perp$ to the direction of the polarization of the excitation light. Therefore the microscope transmission function for the light with different polarizations must be measured.

In the FPA experiments the exciting light coming from the laser is polarized in the plane determined by the direction of the light entering the microscope from the epifluorescence port and the vertical direction. The reflections on the microscope optical components (dichroic beam splitters, mirrors) and the polarization of the excitation light are always in this plane. The fluorescence light from the sample, instead, is partially depolarized and the polarization direction of the fluorescence collected by the photomutiplier can be selected by a Glan–Thompson polarizer. We indicate by two subscripts the polarization of the excited light and the position of the emission polarizer, respectively, measured by the detector. For example, I_{VH} corresponds to vertical polarized excitation light and horizontal position of the emission polarizer. We disregard for the moment the finite size of the excitation volume in which we assume that the polarization of the light is homogenous. For vertically polarized excitation light the observed fluorescence intensities are

$$I_{VV} = k_V S_V I_\parallel,$$
$$I_{VH} = k_V S_H I_\perp, \tag{5}$$

where S_V and S_H are the sensitivities of the microscope front port for the vertically and horizontally polarized components, respectively, and k_V and k_H are proportional to the excitation intensity with parallel and perpendicular polarization that is actually coming onto the sample. The ratio I_{VV}/I_{VH} gives

$$I_{VV}/I_{VH} = G(I_\parallel / I_\perp). \tag{6}$$

To calculate the intensity ratio $I_\parallel / I_\perp$ we need to determine the so-called G factor, $G = S_V / S_H$. Differently from the usual configuration,[71] we cannot use horizontal polarized excitation light in order to get perfectly unpolarized fluorescence, i.e., $I_\parallel = I_\perp$, in Eq. (4). In the present backscattering configuration we exploit the case of horizontally polarized excitation that is now described by the following relations:

$$I_{HH} = k_H S_H I_\parallel,$$
$$I_{HV} = k_H S_V I_\perp. \tag{7}$$

In order to measure the G factor we collect the fluorescence emission for all the four cases described by Eqs. (5), (7), and by combining these equations we obtain

$$G^2 = (I_{VV}/I_{HH})(I_{HV}/I_{VH}),$$
$$(k_V/k_H)^2 = (I_{VV}/I_{HH})(I_{HV}/I_{VH})^{-1}. \tag{8}$$

The rotation of the vertical polarization of the excitation light to the horizontal one is obtained by means of a beam steering and checked by exploiting the reflection of the light on a glass slide at the Brewster angle. The uncertainty on this measurement is $\cong 0.4°$.

As an example on our setup, the measurements on Rhodamine 6G solutions in 60% Glycerol/water give in the range 80–800 MHz a nearly constant value, $G = 0.864 \pm 0.003$ and this has been used to correct all the anisotropy measurements reported here.

We have tested the characterization of the response of the microscope to the light polarization by measuring the FPA decay on protein (Beta-lactoglobulin B) solutions at high dilution corresponding to the limit of $\cong 1$ molecule per excitation volume or less.

We have performed measurements of the fluctuation of the fluorescence, i.e., FCS, and of FPA. The analysis of the fluorescence ACFs provide us directly with the average number of molecules per excitation volume $\cong \kappa / g_F(0)$ that is in the range 0.4–17 (see inset of Figure 9). The average relaxation time $\tau = 210 \pm 20\,\mu s$ corresponds to a diffusion coefficient $D_T \cong 1.15 w_0^2 / 8\tau = 100 \pm 10\,\mu m^2/s$.

The FPA measurements on the same solutions are shown in Figure 10 together with the best-fit functions according to the two-component model described by Eq. (3). The rotational time, $\tau_{ROT} = 9 \pm 1.5$ ns, corresponds to a rotational diffusion coefficient $D_{ROT} = 18 \pm 3$ MHz. The implicit assumption that we have done on the origin of fast relaxation time τ_W is supported by its value (averaged for $C > 100$ nM) $\tau_W = 400 \pm 40$ ps, which could not correspond to the rotational relaxation time of the free dye. In fact, this should be $\cong 200$ ps in water, according to its molecular weight.

The check of the alignment and the polarization response characterization of the setup that we have described above is fulfilled by noticing that the value of the translational diffusion coefficient that is measured by FCS and FPA is in agreement with the size and shape of Beta lactoglubulin (BLG). The computations made by Garcia de la Torre et al.[72] indicate for the dimer form of BLG at $T = 20\,°C$ a value $D_T \cong 78.5\,\mu m^2/s$, that corresponds to $\cong 84\,\mu m^2/s$ at $T \cong 22.5\,°C$. Our experimental estimate $D_T = 100 \pm 10\,\mu m^2/s$ is $\cong 20\%$ larger than the theoretical value and corresponds approximately to the value expected for the monomer of BLG. This discrepancy is due to the fact that most of the BLG dimers have dissociated into monomers at concentrations $C < 280$ nM that corresponds to a mass concentration $\cong 0.01$ g/L. In fact we expect $\cong 90\%$ of BLG monomers in the solution at $C = 280$ nM and at ionic strength $= 50$ mM. Also our estimate of the rotational diffusion coefficient of the Beta-lactoglobulin B by FPA measurements corresponds closely to the prediction that can be done for the monomer of this protein. The theoretical predictions made by Garcia de la Torre et al.[72] for the average rotational diffusion coefficient of the BLG dimer reported at $T \cong 22.5\,°C$ gives $D_{ROT} \cong 8$ MHz. We expect the rotational diffusion of the BLG monomer to be roughly double this figure, since the rotational diffusion scales approximately with the inverse of the molecular volume. The theoretical prediction of $\cong 16$ MHz for the BLG monomer is therefore in good agreement with our experimental estimate $D_{ROT} = 18 \pm 3$ MHz.
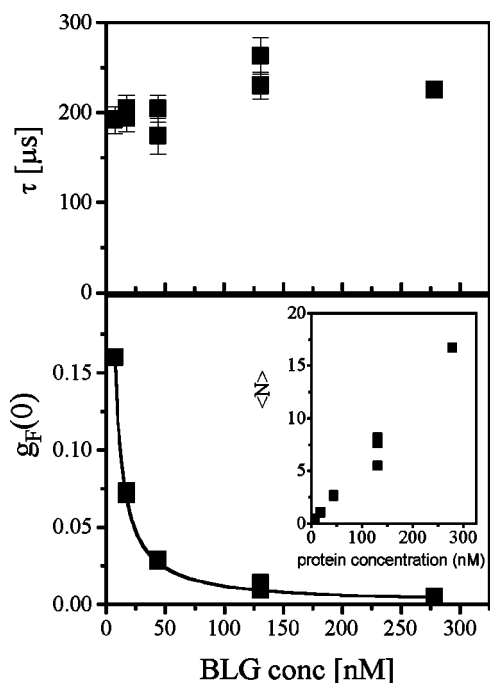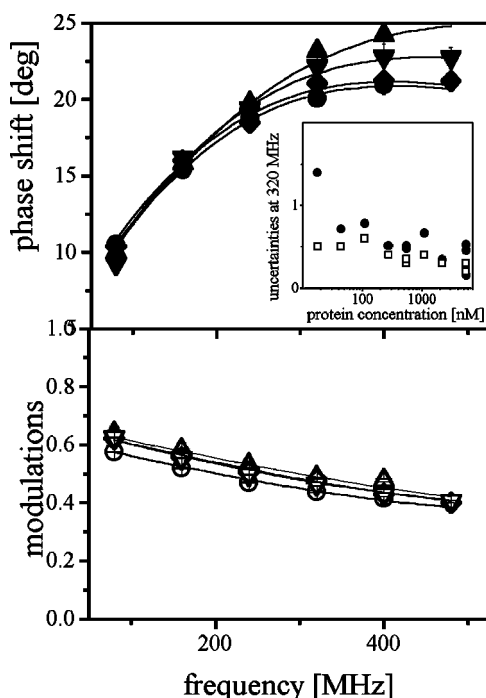
Fig. 9 Result of the analysis of FCS measurements on Beta-lactoglobulin B solutions vs the protein concentration. Upper panel reports the relaxation time, τ. Lower panel shows the zero lag time ACF, $g_F(0)$, together with a fit to Eq. (1) with $B\cong0$. The inset in the lower panel reports the average number of molecules per excitation volume for each concentration.

Fig. 10 Differential phase shifts (upper panel) and polarized modulation ratios (lower panel) spectra for solutions of Beta-lactoglobulin B at protein concentrations $C = 5.5\ \mu M$ (circles), 275 nM (diamonds), 110 nM (down triangles), and 44 nM (up triangles). The solid lines are the best fit of the data according to a two-component model. The inset in the upper panel shows the uncertainty on the differential phase shift (filled circles) and on the polarized modulation ratios (open squares) at 320 MHz to be displayed on the same scale of the phase uncertainties, the uncertainties on the modulations have been multiplied by 100.

We can now compare the estimate of the excitation volumes obtained on the ports for imaging and spectroscopy of the microscope. The PSF of the imaging port corresponds to a three-dimensional Gaussian and from the values of the FWHM lateral and axial resolutions ($w_{r0} = 210 \pm 40$ nm and $z_0 = 700 \pm 50$ nm), we can estimate the excitation volume on the imaging port as $V_{EXC} \cong (\pi/4\ln(2))^{1.5}\, w_{r0}^2 z_0 \cong 0.03 \pm 0.013$ fL.

For both the imaging and the spectroscopy ports the values of the excitation volumes are close to the minimum that can be reached by optical setup. The $\cong 3$ times smaller excitation volume observed for the imaging port is therefore to be ascribed to the different optical paths. For the spectroscopy port a collimated beam fitting the entrance aperture of the objective is used, while in the imaging path a point source is conjugated on the sample plane. We suggest that the parallel use of the two paths for microspectroscopy must be made with caution since the volumes from which the fluorescence is sampled are different in the two ports.

4   Conclusion

TPE microscopy broke into the arena bringing its intrinsic three-dimensional resolution, the absence of background fluorescence, and the charming possibility of exciting ultraviolet excitable fluorescent molecules at infrared wavelengths increasing sample penetration. Moreover, TPE microscopy can be considered an essential imaging system for thick sample and live cell imaging and a powerful setup for the detection of

rarely occurring molecular species and their mutual interaction based on the detection of the fluorescence fluctuations or the lifetime decay time.

At present, the main disadvantages of TPE techniques come from the cost of femtosecond laser sources and the difficulty in predicting or measuring two-photon absorption spectra of the fluorescent molecules potentially utilizable. Because the idea of a TPE microscope is surprisingly straightforward to implement in this paper it has been discussed the conversion of a CLSM to a two-photon multipurpose architecture.[73–84]

References

1. J. N. Gannaway and C. J. R. Sheppard, "Second harmonic imaging in the scanning optical microscope," *Opt. Quantum Electron.* **10**, 435–439 (1978).
2. C. J. R. Sheppard and R. Kompfner, "Resonant scanning optical microscope," *Appl. Opt.* **17**, 2879–2885 (1978).
3. W. Denk, J. H. Strickler, and W. W. Webb, "Two-photon laser scanning fluorescence microscopy," *Science* **248**, 73–76 (1990).
4. T. Wilson and C. J. R. Sheppard, *Theory and Practice of Scanning Optical Microscopy*, Academic, London (1984).
5. M. Gu and C. J. R. Sheppard, "Comparison of three-dimensional

imaging properties between two-photon and single-photon fluorescence microscopy,'' *J. Microsc.* **177**, 128–137 (1995).

6. R. H. Webb, "Confocal optical microscopy," *Rep. Prog. Phys.* **59**, 427–471 (1996).

7. A. Diaspro and C. J. R. Sheppard, "Two-photon excitation fluorescence microscopy," in *Confocal and Two-photon Microscopy: Foundations, Applications and Advances*, A. Diaspro, Ed., Wiley-Liss, Inc., New York (2001).

8. *Handbook of Biological Confocal Microscopy*, J. B. Pawley, Ed., Plenum, New York (1995).

9. S. W. Hell, guest editor, "Non linear optical microscopy," *Bioimaging* **4**(3), 121–224 (1996).

10. A. Diaspro, guest editor, "Two-photon excitation microscopy," *IEEE Eng. Med. Biol. Mag.* **18**(5), 16–99 (1999).

11. A. Diaspro, guest editor, "Two-photon microscopy," *Microsc. Res. Tech.* **47**, 163–212 (1999).

12. *Methods in Cellular Imaging*, A. Periasamy, Ed., Oxford University Press, New York (2001).

13. *Confocal and Two-photon Microscopy: Foundations, Applications and Advances*, A. Diaspro, Ed., Wiley-Liss, Inc., New York (2001).

14. D. Magde and E. L. Elson, "Fluorescence correlation spectroscopy, II. An experimental realization," *Biopolymers* **13**, 29–61 (1974).

15. E. L. Elson and D. Magde, "Fluorescence correlation spectroscopy, I. Conceptual basis and theory," *Biopolymers* **13**, 1–27 (1974).

16. N. L. Thompson, "Fluorescence correlation spectroscopy," in *Topics in Fluorescence Spectroscopy*, J. R. Lakowitz, Ed., Vol. I-Techniques, Chap. 6, p. 337, Plenum, New York (1991).

17. P. Schwille, J. Bieschke, and F. Oehlenschlager, "Kinetic investigation by fluorescence correlation spectroscopy—the analytical and diagnostic potential of diffusion studies," *Biophys. Chem.* **66**, 211–228 (1997).

18. J. R. Lakowicz, "Fluorescence polarization," in *Principles of Fluorescence Spectroscopy*, p. 131, Plenum, New York (1991).

19. T. W. J. Gadella, T. M. Jovin, and R. M. Clegg, "Fluorescence lifetime imaging microscopy (FLIM)-spatial resolution of microstructures on the nanosecond time-scale," *Biophys. Chem.* **48**, 221–239 (1993).

20. P. T. C. So, K. M. Berland, T. French, C. Y. Dong, and E. Gratton, "Two photon fluorescence microscopy: Time resolved and intensity imaging," in *Fluorescence Imaging Spectroscopy and Microscopy*, X. F. Wang and B. Herman, Eds., Chemical Analysis Series, Vol. 137, pp. 351–373, Wiley, New York (1996).

21. J. Sytsma, J. Vroom, H. C. Gerritsen, and Y. K. Levine, "Development of a confocal laser scanning fluorescence microscope using two-photon excitation in combination with time gated detection," *Proc. SPIE* **2412**, 110–114 (1995).

22. K. M. Berland, P. T. So, Y. Chen, W. W. Mantulin, and E. Gratton, "Scanning two-photon fluctuation correlation spectroscopy: particle counting measurements for detection of molecular aggregation," *Biophys. J.* **71**, 410–420 (1996).

23. A. Squire, P. J. Verveer, and P. I. H. Bastiaens, "Multiple frequency fluorescence lifetime imaging microscopy," *J. Microsc.* **197**, 136–149 (2000).

24. D. E. Spence, P. N. Kean, and W. Sibbett, "60-fsec pulse generation from a self-mode-locked Ti:sapphire laser," *Opt. Lett.* **16**, 42–45 (1991).

25. E. Gratton and M. J. van de Ven, Laser sources for confocal microscopy, in *The Handbook of Biological Confocal Microscopy*, J. Pawley, Ed., pp. 69–97, Plenum, New York (1995).

26. W. G. Fisher, E. A. Watcher, M. Armas, and C. Seaton, "Titanium: sapphire laser as an excitation source in two-photon spectroscopy," *Appl. Spectrosc.* **51**(2), 218–226 (1997).

27. A. Diaspro, "Building a two-photon microscope using a laser scanning confocal architecture," in *Methods in Cellular Imaging*, A. Periasamy, Ed., pp. 162–179, Oxford University Press, New York (2001).

28. A. Majewska, G. Yiu, and R. Yuste, "A custom-made two-photon microscope and deconvolution system," *Pflugers Archiv-Eur. J. Physiol.* **441**(2/3), 398–408 (2000).

29. W. Denk, D. W. Piston, and W. W. Webb, "Two-photon molecular excitation in laser scanning microscopy," in *The Handbook of Biological Confocal Microscopy*, J. Pawley, Ed., pp. 445–458, Plenum, New York (1995).

30. S. M. Potter, C. M. Wang, P. A. Garrity, and S. E. Fraser, "Intravital imaging of green fluorescent protein using 2-photon laser-scanning microscopy," *Gene* **173**, 25–31 (1996).

31. K. Konig, H. Liang, M. W. Berns, and B. J. Tromberg, "Cell damage in near infrared multimode optical traps as a result of multiphoton absorption," *Opt. Lett.* **21**, 1090–1092 (1996).

32. C. Soeller and M. B. Cannell, "Construction of a two-photon microscope and optimisation of illumination pulse duration," *Pflugers Arch.* **432**, 555–561 (1996).

33. A. Periasamy, P. Skoglund, C. Noakes, and R. Keller, "An evaluation of two-photon excitation versus confocal and digital deconvolution fluorescence microscopy imaging in Xenopus morphogenesis," *Microsc. Res. Tech.* **47**, 172–181 (1999).

34. C. Soeller and M. B. Cannell, "Two-photon microscopy: Imaging in scattering samples and three dimensionally resolved flash photolysis," *Microsc. Res. Tech.* **47**, 182–195 (1999).

35. A. Diaspro, M. Corosu, P. Ramoino, and M. Robello, "Adapting a compact confocal microscope system to a two-photon excitation fluorescence imaging architecture," *Microsc. Res. Tech.* **47**, 196–205 (1999).

36. R. Gauderon, P. B. Lukins, and C. J. R. Sheppard, "Effect of a confocal pinhole in two-photon microscopy," *Microsc. Res. Tech.* **47**, 210–214 (1999).

37. P. Torok and C. J. R. Sheppard, "The role of pinhole size in high aperture two and three-photon microscopy," in *Confocal and Two-Photon Microscopy: Foundations, Applications and Advances*, A. Diaspro, Wiley-Liss, Inc., New York (2001).

38. M. Gu and C. J. R. Sheppard, "Effects of a finite sized pinhole on 3D image formation in confocal two-photon fluorescence microscopy," *J. Mod. Opt.* **40**, 2009–2024 (1993).

39. M. Eherneberg and R. Rigler, "Rotational Brownian motion and fluorescence intensity fluctuations," *Chem. Phys.* **4**, 390–401 (1974).

40. S. R. Aragon and R. Pecora, "Theory of dynamic light scattering from large anisotropic particles," *J. Chem. Phys.* **66**, 2506–2516 (1977).

41. H. Quian and E. L. Elson, "Analysis of confocal laser-microscope optics for 3-D fluorescence correlation spectroscopy," *Appl. Opt.* **30**, 1185 (1991).

42. R. Rigler, U. Mets, J. Windengren, and P. Kask, "Fluorescence correlation spectroscopy with high count rate and low background: analysis of translational diffusion," *Eur. Biophys. J.* **22**, 169–175 (1993).

43. D. E. Koppel, F. Morgan, A. E. Cowan, and J. H. Carson, "Scanning concentration correlation spectroscopy using the confocal laser microscope," *Biophys. J.* **66**, 502–507 (1994).

44. Y. Chen, J. D. Muller, P. T. C. So, and E. Gratton, "The photon counting histogram in fluorescence fluctuation spectroscopy," *Biophys. J.* **77**(1), 553–567 (1999).

45. B. Saleh, *Photoelectron Statistics, with Applications to Spectroscopy and Optical Communications*, Springer, Berlin (1978).

46. H. Quian and E. L. Elson, "Distribution of molecular aggregation by analysis of fluctuation moments," *Proc. Natl. Acad. Sci. U.S.A.* **85**, 5479–5483 (1990).

47. J. D. Müller, Y. Chen, and E. Gratton, "Resolving heterogeneity on the single molecular level with the photon-counting histogram," *Biochem. J.* **78**, 474–486 (2000).

48. J. Girkin and D. Wokosin, "Practical multiphoton microscopy," in *Confocal and Two-photon Microscopy: Foundations, Applications and Advances*, A. Diaspro, Ed., Wiley-Liss, Inc., New York (2001).

49. A. Schönle and S. W. Hell, "Heating by absorption in the focus of an objective lens," *Opt. Lett.* **23**, 325 (1998).

50. K. Konig, "Multiphoton microscopy in life sciences," *J. Microsc.* **200**, 83–104 (2000).

51. K. Konig and U. K. Tirlapur, "Cellular and subcellular perturbations during multiphoton microscopy," in *Confocal and Two-Photon Microscopy: Foundations, Applications and Advances*, A. Diaspro, Ed., Wiley-Liss, Inc., New York (2001).

52. R. Wolleschensky, M. Dickinson, and S. E. Fraser, "Group velocity dispersion and fiber delivery in multiphoton laser scanning microscopy," in *Confocal and Two-Photon Microscopy: Foundations, Applications and Advances*, A. Diaspro, Ed., Wiley-Liss, Inc., New York (2001).

53. M. Stanley, "Improvements in optical filter design," *Proc. SPIE* **4240**, (2001).

54. M. Ghioni, S. Cova, F. Zappa, and C. Samori, "Compact active quenching circuit for fast photon counting with avalanche photodiodes," *Rev. Sci. Instrum.* **67**(10), 3440–3448 (1996).

55. *Confocal Microscopy*, T. Wilson, Ed., *Academic*, London (1990).

56. J. Jonkman and E. Stelzer, "Resolution and contrast in confocal and

two-photon microscopy," in *Confocal and Two-photon Microscopy: Foundations, Applications and Advances*, A. Diaspro, Ed., Wiley-Liss, Inc., New York (2001).

57. G. Chirico, F. Olivini, and S. Beretta, "Fluorescence excitation volume in two-photon microscopy by autocorrelation spectroscopy and photon counting histogram," *Appl. Spectrosc.* **54**(7), 1084–1090 (2000).

58. C. Xu, W. Zipfel, J. B. Shear, R. M. Williams, and W. W. Webb, "Multi-photon fluorescence excitation: new spectral windows for biological nonlinear microscopy," *Proc. Natl. Acad. Sci. (U.S.A.)* **93**, 10763–10768 (1996).

59. C. Xu and W. W. Webb, "Measurement of two-photon excitation cross sections of molecular fluorophores with data from 690 to 1050 nm," *J. Opt. Soc. Am.* **13**, 481–491 (1996).

60. P. E. Hanninen and S. W. Hell, "Femtosecond pulse broadening in the focal region of a two-photon fluorescence microscope," *Bioimaging* **2**, 117–121 (1994).

61. M. Muller, J. Squier, and G. J. Brakenhoff, "Measurements of femtosecond pulses in the focal point of a high numerical aperture lens bt two-photon absorption," *Opt. Lett.* **20**, 1038–1040 (1995).

62. A. Diaspro, S. Annunziata, M. Raimondo, P. Ramoino, and M. Robello, "A single-pinhole CLSM for 3-D imaging of biostructures," *IEEE Eng. Med. Biol. Mag.* **18**(4), 106–110 (1999).

63. A. Diaspro, S. Annunziata, M. Raimondo, and M. Robello, "Three-dimensional optical behavior of a confocal microscope with single illumination and detection pinhole through imaging of subresolution beads," *Microsc. Res. Tech.* **45**(2), 130–131 (1999).

64. R. Y. Tsien and Y. Wagonner, "Fluorophores for confocal microscopy," in *Handbook of Biological Confocal Microscopy*, 2nd ed., Ch. 16, p. 267, Plenum, New York (1995).

65. B. Bianco and A. Diaspro, "Analysis of the three dimensional cell imaging obtained with optical microscopy techniques based on defocusing," *Cell Biophys.* **15**, 189–200 (1989).

66. O. Nakamura, "Three-dimensional imaging characteristics of laser scan fluorescence microscopy: Two-photon excitation vs. single-photon excitation," *Optik (Stuttgart)* **93**, 39–42 (1993).

67. G. H. Patterson and D. W. Piston, "Photobeleaching in two-photon excitation microscopy," *Biophys. J.* **78**, 2159–2162 (2000).

68. K. M. Berland, P. T. C. So, and E. Gratton, "Two-photon fluorescence correlation spectroscopy: method and application to the intracellular environment," *Biophys. J.* **68**, 694 (1995).

69. J. M. Beechem and E. Gratton, "Fluorescence spectroscopy data analysis environment: a second generation global analysis program," *Proc. SPIE* **909**, 70 (1988).

70. R. F. Steiner, *Fluorescence Anisotropy: Theory and Applications in Topics in Fluorescence Spectroscopy: Principles*, Vol. 2, J. R. Lakowicz, Ed., Plenum, New York (1991).

71. J. R. Lakowicz, "Fluorescence polarization," in *Principles of Fluorescence Spectroscopy*, p. 125, Plenum, New York (1991).

72. J. Garcia de la Torre, M. L. Huertas, and B. Carrasco, "Calculation of hydrodynamic properties of globular proteins from their atomic-level structure," *Biophys. J.* **78**, 719 (2000).

73. M. Albota et al., "Design of organic molecules with large two-photon absorption cross sections," *Science* **281**, 1653–1656 (1998).

74. G. Baldini, S. Beretta, G. Chirico, H. Franz, E. Maccioni, P. Mariani, and F. Spinozzi, "Salt induced association of Beta-lactoglobulin studied by salt light and X-ray scattering," *Macromolecules* **32**, 6128 (1999).

75. V. E. Centonze and J. G. White, "Multiphoton excitation provides optical sections from deeper within scattering specimens than confocal imaging," *Biophys. J.* **75**, 2015–2024 (1998).

76. W. Denk, "Two-photon excitation in functional biological imaging," *J. Biomed. Opt.* **1**, 296–304 (1996).

77. A. Diaspro and M. Robello, "Two-photon excitation of fluorescence in three-dimensional microscopy," *Eur. J. Histochem.* **43**(3), 70–79 (1999).

78. T. Furuta, S. S.-H. Wang, J. L. Dantzker, T. M. Dore, W. J. Bybee, E. M. Callaway, W. Denk, and R. Y. Tsien, "Brominated 7-hydroxycoumarin-4-ylmethyls: Photolabile protecting groups with biologically useful cross-sections for two photon photolysis," *Proc. Natl. Acad. Sci. U.S.A.* **96**, 1193–1200 (1999).

79. S. W. Hell, K. Bahlmann, M. Schrader, A. Soini, H. Malak, I. Gryczynski, and J. R. Lakowicz, "Three-photon excitation in fluorescence microscopy," *J. Biomed. Opt.* **1**, 71–74 (1996).

80. H. J. Koester, D. Baur, R. Uhl, and S. W. Hell, "Ca2+ fluorescence imaging with pico- and femtosecond two-photon excitation: Signal and photodamage," *Biophys. J.* **77**, 2226–2236 (1999).

81. K. König, P. T. C. So, W. W. Mantulin, and E. Gratton, "Cellular response to near-infrared femtosecond laser pulses in two-photon microscopes," *Opt. Lett.* **22**, 135–136 (1997).

82. K. König, T. W. Becker, P. Fischer, I. Riemann, and K. J. Halbhuber, "Pulse-length dependence of cellular response to intense near-infrared laser pulses in multiphoton microscopes," *Opt. Lett.* **24**, 113–115 (1999).

83. E. H. K. Stelzer, S. Hell, and S. Lindek, "Nonlinear absorption extends confocal fluorescence microscopy into the ultra-violet regime and confines the illumination volume," *Opt. Commun.* **104**, 223–228 (1994).

84. D. W. Wokosin, V. E. Centonze, S. Crittenden, and J. G. White, "Three-photon excitation fluorescence imaging of biological specimens using an all-solid-state laser," *Bioimaging* **4**, 208–214 (1996).